Materials Horizons

ROYAL SOCIETY OF CHEMISTRY

COMMUNICATION

View Article Online
View Journal | View Issue

Cite this: *Mater. Horiz.*, 2024, **11**, 2718

Received 21st November 2023,
Accepted 4th March 2024

DOI: 10.1039/d3mh01976d

rsc.li/materials-horizons

Upcycling plastic waste into fully recyclable composites through cold sintering†

Po-Hao Lai,[a] Shelby L. Hall,[a] Yi-Chen Lan,[a] Jia-Ruey Ai,[a] Arian Jaberi,[a] Amir Sheikhi,[a] Rui Shi,[a] Bryan D. Vogt *[a] and Enrique D. Gomez *[ab]

Plastics have substantial societal benefits, but their widespread use has led to a critical waste management challenge. While mechanical recycling dominates the reuse of post-consumer plastics, it is limited in efficacy, especially for composites. To address this, we propose a direct reprocessing approach that enables the creation of hybrid, long-lasting, and durable composites from difficult-to-recycle plastics. This approach utilizes cold sintering, a process that consolidates inorganic powders through fractional dissolution and precipitation at temperatures far below conventional sintering; these temperatures are compatible with plastic processing. We show that this process can create inorganic-matrix composites with significant enhancements in tensile strength and toughness over pure gypsum, which is commonly found in construction waste. These composites can be recycled multiple times through direct reprocessing with the addition of only water as a processing promoter. This approach to recycling leads to composites with orders of magnitude lower energy demand, global warming potential, and water demand, when compared against common construction products. Altogether, we demonstrate the potential for cold sintering to integrate waste into high-performance recyclable composites.

New concepts

We present a novel concept for upcycling of construction waste, including plastics, by utilizing cold-sintering, a method developed to densify ceramics at low temperatures (<200 °C). We showcase its application using commonly available waste materials like polypropylene (PP) and gypsum. This approach distinguishes itself by addressing the drawbacks of traditional mechanical recycling, specifically averting the decline in mechanical properties typically associated with downcycling practices. In comparison with existing research that has employed cold-sintering for composite production typically towards device applications, our work demonstrates the use of this method to repurpose and upcycle plastic waste for the first time. Furthermore, this work is also the first demonstration of cold-sintering to manufacture tailored tensile test specimens, which will expand the potential for diversifying testing procedures of cold sintering samples. Additionally, our life cycle assessment quantitatively uncovers the substantially reduced environmental impact of the reprocessed cold-sintered composite compared to commonplace building materials. Even when using virgin feedstocks, cold sintering displays lower energy requirements and decreased global warming potential, underscoring its efficacy in processing recyclable composites. This study represents a step forward in sustainable materials, promising to elevate circularity within the domain of materials science.

Introduction

Since the 1950s, plastic has revolutionized the way we live by providing convenient and versatile products that have become ubiquitous in our daily lives. Despite its undeniable benefits, the disposal of plastic has become a critical issue, with the constant generation of plastic waste causing significant environmental and health problems worldwide.[1–3] Traditional methods of plastic waste management, such as landfill and incineration, are not sustainable solutions due to their adverse impacts on the environment and human health.[4–7] As a result, identifying effective ways to manage plastic waste has become a pressing concern for policymakers, scientists, and the public.

In recent years, mechanical recycling has gained widespread acceptance as a pivotal approach to address the pressing issue of plastic waste. This method holds several benefits, such as in reducing the environmental footprint of plastics, conserving valuable resources, and diverting plastics from overflowing landfills. Moreover, it plays a substantial role in promoting sustainability and advancing circular economy principles, and in highlighting the growing importance of plastic recycling throughout our society.[5] Nonetheless, despite its merits, mechanical recycling faces substantial challenges, especially when dealing with polypropylene (PP) due to its propensity for

[a] *Department of Chemical Engineering, The Pennsylvania State University, University Park, PA 16802, USA. E-mail: bdv5051@psu.edu, edg12@psu.edu*
[b] *Department of Material Science and Engineering, The Pennsylvania State University, University Park, PA 16802, USA*

† Electronic supplementary information (ESI) available. See DOI: https://doi.org/10.1039/d3mh01976d

chain scission during processing.[8] Conventional mechanical recycling techniques often grapple with a fundamental constraint: they tend to result in a phenomenon referred to as downcycling. The recycling process leads to a gradual reduction in the quality and performance of plastics with each successive recycling cycle.[5,9–11] Consequently, the introduction of impurities and reprocessing itself lead to a decline in plastic mechanical properties.[12] This inherent limitation poses a significant obstacle, particularly for PP, a ubiquitous plastic that experiences a rapid deterioration in performance and quality with recycling. Although chemical or advanced recycling has been gaining momentum as an alternative for plastic mechanical recycling,[13] the breakdown of the plastic back to its basic building blocks has disadvantages in the loss of the embedded energy in the original production of the polymer.[9] This embodied energy is also a substantial contribution to the environmental footprint of many inorganic components used in the building and construction industry, where movement towards circularity of building materials is a key route to achieving sustainability.[14]

Cold sintering is a recently developed approach to densify ceramics.[15] Unlike traditional sintering, cold sintering uses a liquid phase to undergo dissolution and precipitation of a vanishingly small fraction of the ceramic to fuse powders at much lower sintering temperatures (<200 °C).[16–22] Cold sintering enables densification to $>99\%$ under appropriate processing conditions.[23] Even with minimal dissolution in the transient solvent, cold sintering provides the possibility to co-sinter ceramics, organics, and polymers in one step.[24,25] Previous work has demonstrated unique composites made from salt and ceramic materials,[26] layered structures,[27] and metals.[28] As such, cold sintering provides the potential to integrate plastic waste with various other materials and likely opportunities for enhancing the sustainability of composite materials. The ability to sinter inorganic phases at modest temperatures opens the door for reprocessability, in a manner not typically possible for plastic composites.

In this study, we focus on developing an approach for creating structural materials from plastic waste and construction waste by cold sintering polypropylene (PP) with $CaSO_4$, which is the main component in gypsum drywall. We demonstrate that this approach results in a range of compositions (14–68 vol% PP) with promising mechanical behavior. Cold sintered PP/$CaSO_4$ inorganic matrix composites can exhibit ductility under tensile deformation, in contrast to the extreme brittle failure that is typical of gypsum alone. Moreover, the modest processing temperature of cold sintering precludes chain scission and polymer degradation after reprocessing,[29,30] enabling re-sintering of ground composites multiple times without any significant degradation in mechanical properties. As a demonstration, we show synthesis of composites that include actual plastic waste and exhibit similar mechanical properties as when pristine materials are used. Quantification of the environmental impact through life cycle assessment calculations reveals that cold sintered composites exhibit significantly lower energy demand, global warming potential, and water demand when compared to values for alternative building materials (particle board, strand board, sawn timber, and gypsum board). Imparting recyclability to cold sintered composites further decreases our impact metrics by orders of magnitude. Our work shows the potential for cold sintering to enhance sustainability by upcycling plastic waste into recyclable composites towards use in structural applications.

Results and discussions

Cold sintered $CaSO_4$/PP composite

Although some plastics, such as polyethylene terephthalate (PET), are recycled at modest rates (18% for PET), PP waste is seldom recycled, with rates $<1\%$ in the US.[31] In addition, construction waste is currently about twice as large by mass as municipal waste,[32] which underscores the substantial volume generated within the construction industry. Gypsum, a widely used constituent in construction, contributes to this large volume of construction waste as drywall, wallboard, or plasterboard, which are often used for wall and ceiling finishes. Gypsum exhibits attributes that facilitate easy installation, disassembly, and potential for recycling at the end of its lifecycle.[33,34] We thus focused our initial demonstration on composites made from PP and gypsum ($CaSO_4$). Ground polypropylene particles (250–500 μm) were mixed with powders of $CaSO_4$ and 10 wt% deionized water (of total powder mass). The moistened powders were loaded into a 316 Stainless steel mold of type V tensile bars (ASTM D638). Cold sintering then took place at 160 °C and 200 MPa for 1 h under ambient conditions as these conditions provide for sufficient flow of PP, appropriate duration for plateau in the sintered composite density and avoid deformation of the mold. Samples are labeled with the polypropylene content as PP-x, where x is the percent PP by volume. More details on procedures and selection of processing parameters for composite fabrication can be found in the Materials and methods section.

Ceramics are known for their exceptional compressive strength and hardness while exhibiting poor tensile properties.[35] In fact, the low tensile strength of ceramics is a significant limitation in some applications. Uniaxial tensile testing of ceramics is notably scarce in literature[36] due to the inherent difficulty in forming suitable specimens and conducting such tests. In this study, we demonstrate a novel approach using cold sintering techniques, which has been noted to enhance the mechanical properties of ceramic materials.[37,38] This method has enabled the fabrication of integral tensile bars for ceramic matrix composites and has facilitated their subsequent testing. Moreover, properties of plastic composites are typically limited by the aggregation of fillers at high loadings. The small, but finite solubility of $CaSO_4$ in water alters the mechanism by which the morphology of the composite develops. Fig. 1(a) schematically highlights how the addition of water as a processing, transient solvent alters the structure of the composite and leads to significant strengthening. The dissolution–precipitation of $CaSO_4$ leads to an inorganic framework in the composite to lock the $CaSO_4$ structure, while the processing temperature

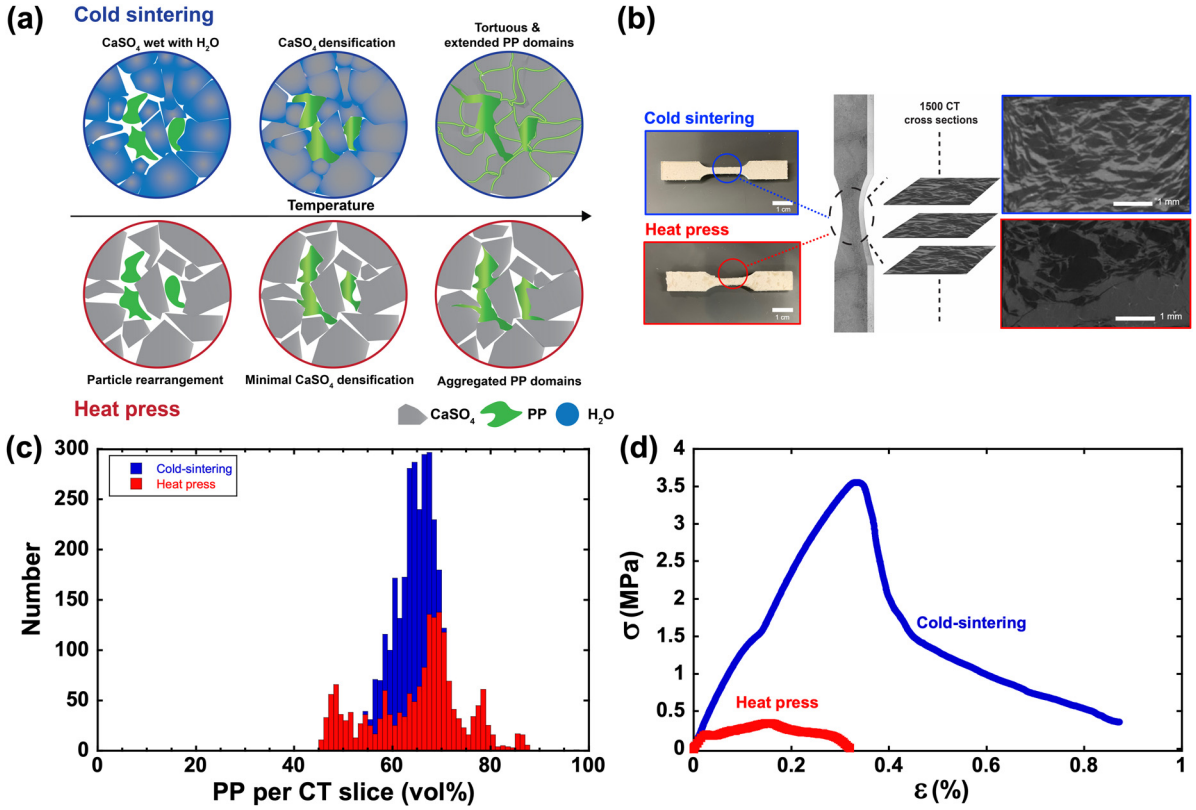

Fig. 1 (a) Schematic comparing cold sintering and heat pressing to fabricate $CaSO_4$/PP composites. (b) Images of cold sintered and heat pressed composites containing 68.2 vol% of PP (left) and the cross-section morphology from μCT (right). The PP region appears as a lower gray scale value (black), distinct from the $CaSO_4$ region (gray). (c) Histogram of local composition of cross-sections from μCT analysis for the two processing routes. (d) Representative stress–strain behavior of 68.2 vol% of PP composites from cold sintering and heat press processing.

enables flow of PP between the $CaSO_4$ particles to produce tortuous PP extended domains within the composite as the material densifies during sintering (Fig. 1(b)). This enables the $CaSO_4$/PP composite to densify during the cold sintering process, as shown in Fig. S1 (ESI†). Without water, pressing the composite at the same conditions leads an aggregated composite structure due to the mobility of PP, the freedom of the $CaSO_4$ particles, and poor interfacial interactions between PP and $CaSO_4$, as expected (Fig. 1(b)).

These differences impact the macroscopic appearance of the $CaSO_4$/PP composite tensile specimens. The cold-sintered specimen appears homogeneous from visual examination, while aggregated regions can be identified by eye in the heat pressed sample (Fig. 1(b)). A cross section from X-ray microcomputed tomography (μCT) in the gauge region of the sample illustrates this difference at the microscale. A statistical analysis of the full specimen quantifies the distribution of components to more clearly illustrate the heterogeneity. Fig. 1(c) shows the histogram of PP concentration across the gauge region from individual μCT cross sections. As the overall composition is identical, the average composition is not dependent on the methodology for generating the specimen. Cold sintering leads to a narrow distribution in composition, while the heat pressed sample has a broader distribution due to substantial number of domains with nearly 50% excess or deficit in PP.

The difference in morphology and homogeneity with processing method significantly impacts the response to tensile deformation, as shown in Fig. 1(d). The Young's modulus is 30% higher with cold sintering (1473 MPa) than after heat press processing (1112 MPa) despite the similarity in processing (except the use of water in cold sintering). More strikingly, the ultimate tensile stress (UTS) is 8 times larger with cold sintering (3.55 MPa) than hot pressing (0.43 MPa) despite identical materials and processing conditions, again except the inclusion of water for cold sintering. The increased strength does not come at the expense of the toughness; the cold sintered material is more ductile, with the strain at break nearly 3 times larger than samples made with a heat press. These results illustrate the unique composite structures and properties that can be obtained with cold sintering.

Mechanical and morphological properties

To gain deeper insights into the tensile characteristics of $CaSO_4$/PP composites, we conducted a comprehensive analysis of the stress–strain behavior for composites spanning a broad spectrum of PP concentrations, ranging from 0 vol% to 68.2 vol%. The findings are presented in Fig. 2. As the proportion of PP increases, the stress–strain responses of the $CaSO_4$/PP composites undergoes a remarkable transformation from brittle to ductile failure modes. In Fig. 2(a), for instance,

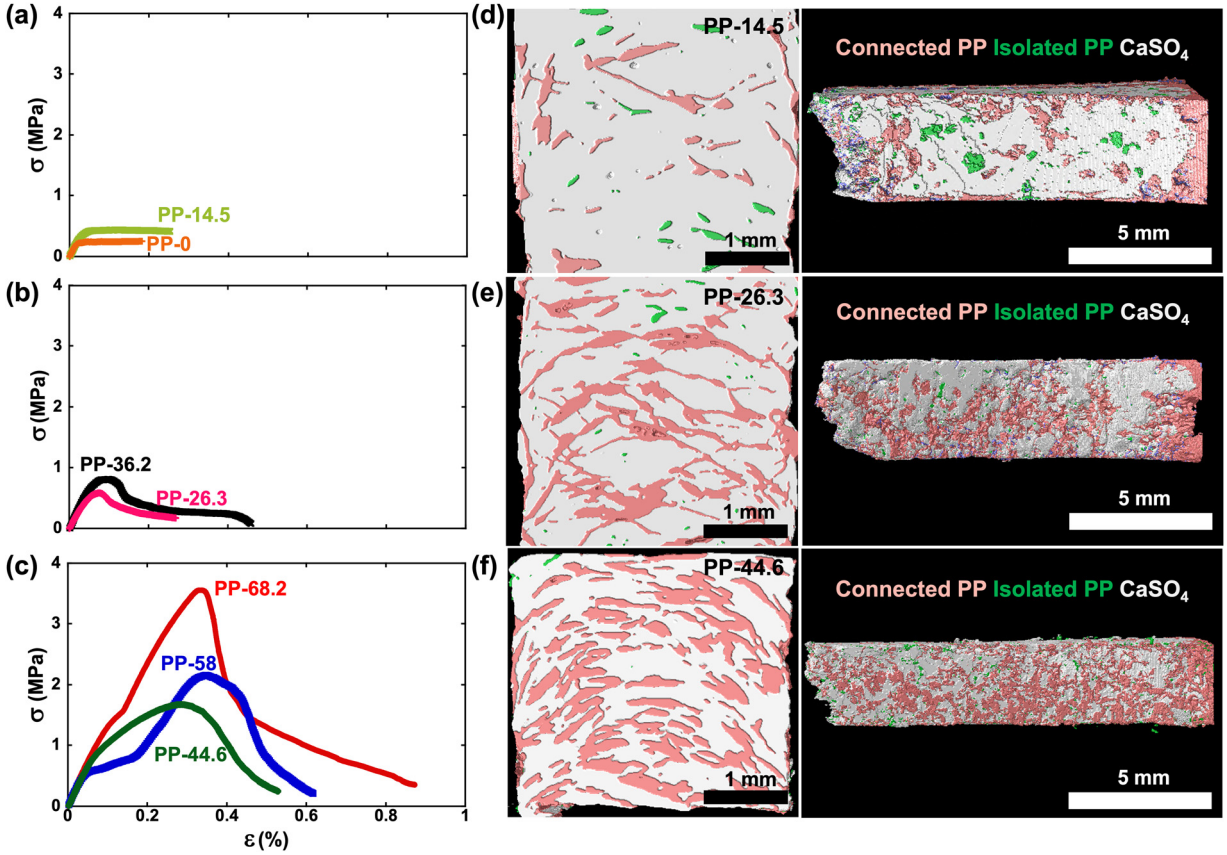

Fig. 2 Representative stress–strain curves at (a) low, (b) medium and (c) high PP content and connectivity analysis of μ-CT images for (d) PP-14.5, (e) PP-26.3, and (f) PP-44.6. The false color allows for identification of connected PP (pink) and isolated PP (green) phases within the composite.

PP-14.5 (14.5 vol% of PP) exhibits a stress–strain curve closely resembling that of PP-0, which represents the tensile behavior of pure $CaSO_4$. In both cases, PP-0 and PP-14.5, a brittle mode of failure was observed, characterized by immediate sample rupture upon reaching the ultimate tensile stress (UTS) without any noticeable plastic deformation. At volume fractions of PP exceeding 25 vol%, the stress–strain curves of PP-26.3 and PP-36.2 in Fig. 2(b) show a distinctive strain-softening behavior of composites.[39,40] This behavior is characterized by a continuous and gradual decline in stress following the attainment of the UTS, which is indicative of a transition from a brittle to quasi-brittle material response.[39] Further increasing the PP content in the composite leads to a noticeable shift in behavior, as shown in Fig. 2(c). For instance, PP-58 demonstrates a pivotal transition at approximately 0.1% strain, coinciding with the initial cracking of the $CaSO_4$ matrix. As successive matrix cracks form within $CaSO_4$, the composite undergoes a transition with a substantial increase in the ultimate tensile stress. This is followed by strain softening, ultimately culminating in fracture at an elevated tensile strain. This transition from brittle to ductile behavior is intrinsically linked to morphological alterations within the composite.

From the qualitative visual examination of the internal morphology, there are clear differences that correlate with the mechanical properties. As depicted in Fig. 2(d)–(f), these images offer valuable insights into the phases and their connectivity. The brittleness observed in PP-14.5 is attributed to findings from the μ-CT cross-sectional analysis (Fig. 2(d)), which highlights that the limited presence of PP was insufficient to sustain the tensile bar when the inherently brittle $CaSO_4$ material fails under stress. This brittleness marks a clear mechanical behavior. Conversely, a transition from brittle to quasi-brittle material behavior becomes apparent in the morphological shifts visible in the μ-CT cross section of PP-26.3 (Fig. 2(e)). In this instance, a more significant presence of interconnected PP forms a structural framework resembling fibrils, in contrast to the random dispersion of PP observed in PP-14.5. The prevalence of abundant, interconnected PP fibrils within the $CaSO_4$/PP composites contributes to enhanced ductility during tensile testing, signifying a transition towards ductile behavior. This shift from quasi-brittle to ductile behavior is intrinsically linked to the morphological alterations within the composite. As depicted in Fig. 2(f), the abundant PP enables the retention of the tensile bar, even as multiple $CaSO_4$ matrix cracks develop due to the lower UTS of $CaSO_4$. The remaining PP matrix allows the composite to withstand stretching, subsequently undergoing apparent strain hardening and softening during uniaxial tensile testing. This transformation further reinforces the composite, ultimately enhancing its ultimate stress and elongation capabilities.

The tensile properties of composites are influenced by the filler volume fraction,[41] filler dispersion and distribution,[42] and connectivity of the filler.[43] The reconstruction of the 3D morphology from μCT enables slices of the composite to be quantified individually to provide both average and variance in properties. Table 1 summarizes the average composite composition from each cross-section. The composition agrees with the original loading, and the standard deviation is relatively low, indicative of a homogeneous distribution along the specimens at the macroscopic scale. The histograms of these distributions are shown in Fig. S2 (ESI†). Moreover, the average composition of each slice from μCT fluctuates along the length of the tensile bars, as depicted in Fig. S3 (ESI†), but these variations are generally smaller than approximately 5 vol% PP. Thus, the local heterogeneity in the composites is smaller than the compositional differences of the composites examined and the differences in the mechanical response between compositions is likely dominated by perturbations to the morphology.

Table 1 Compositions and connectivity of cold sintered composites from μ-CT analysis

	PP-14.5	PP-26.3	PP-44.6
PP composition as loaded (vol%)	14.5	26.3	44.6
PP calculated from μCT (vol%)	14.3 ± 2.5	27.4 ± 2.3	44.5 ± 2.6
Connectivity of PP (%)	80.4 ± 6.7	98.5 ± 1.4	99.7 ± 0.2

Nevertheless, due to the sensitivity of tensile tests to local structures, the heterogeneity in the composites also likely contributes to the variance in the mechanical response between replicates.

In addition to the composition, the phase connectivity impacts the tensile response.[16] Fig. 2 also illustrates that the number of the isolated PP domains decreases as the PP content increases. Roughly 20% of the PP in the PP-14.5 is isolated, but this decreases to <1.5% for PP-26.3. This increased connectivity of the PP appears correlated with the yielding behavior and can be rationalized in terms of the effectiveness of the PP phase in carrying the stress relative to fracture of the $CaSO_4$ phase. Nevertheless, a small increase in the connectivity for PP-44.6 leads to a much more extensible and ductile composite, so other morphological factors are critical in determining the tensile response of the cold sintered composite.

Fig. S4 and S5 (ESI†) show how the tensile properties of the cold sintered $CaSO_4$/PP composites depend on the composition. The UTS of $CaSO_4$/PP composites increases with PP content as shown in Fig. S5(a) (ESI†) but the UTS appears to increase more when the PP volume fraction is >40 vol%. This larger increase in the UTS at higher PP content is consistent with a matrix transition of this $CaSO_4$/PP composite, from effectively a ceramic matrix to one where the polymeric content is sufficient for a continuous reinforcement that reduces the propensity for crack propagation. This speculation is supported

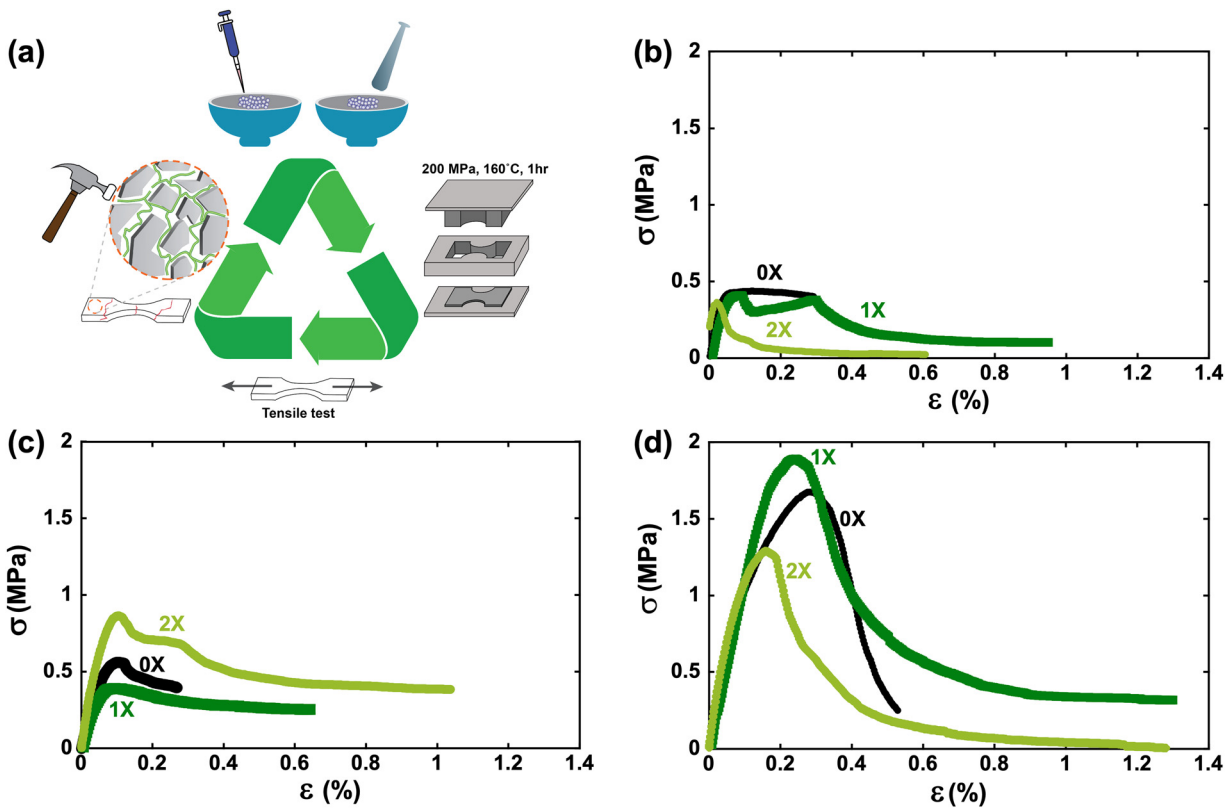

Fig. 3 Reprocessing of $CaSO_4$/PP composites. (a) Schematic illustrating the reprocessing of the composites where cold sintered materials are mechanically ground and cold sintered with the addition of only water. Representative stress–strain curves for (b) PP-14.5, (c) PP-26.3, and (d) PP-44.6 for pristine (0×) and materials recycled 1× and 2×.

by analysis of the $CaSO_4$ connected regions from μ-CT, where the largest connected $CaSO_4$ region is shown in red in Fig. S5(a) (ESI†). When PP is <40 vol%, the $CaSO_4$ is almost all connected within the composite. Nevertheless, the largest connected $CaSO_4$ region decreases significantly at higher PP content; with this morphology, the PP can act to dampen or blunt cracks in $CaSO_4$.

Fig. S5(b) (ESI†) illustrates the elongation at yield for the $CaSO_4$/PP composites. The elongation at yield is essentially unchanged until the PP content is >40 vol%, which is consistent with the smaller $CaSO_4$ domains reducing the propensity for crack propagation. The Young's modulus is only modestly impacted by the PP content with a small increase in modulus with increasing PP content, which we attribute to the fracture of the $CaSO_4$ phase, as the cold sintered inorganic exhibits a lower modulus than the compression molded PP. The low experimentally measured modulus for $CaSO_4$ (*ca.* 1 GPa) is lower than expected for pure gypsum, suggesting some porosity is present,[44] although the determined modulus is consistent with some other mechanical properties reported in the literature for $CaSO_4$.[45] When the volume fraction of PP is $<$ 40 vol%, the Young's modulus is closer to that of cold sintered $CaSO_4$, while the Young's modulus of composites at high PP loadings is closer to the value of pristine PP. These results point towards key structural characteristics for enhancements in the properties of inorganic–organic composites.

Reprocessing of $CaSO_4$/PP composites

We also demonstrate an approach to recycle PP/$CaSO_4$ composites through cold sintering. As shown in Fig. 3(a), we take samples used in tensile tests and re-grind them for subsequent cold sintering into reprocessed $CaSO_4$/PP composites. Fig. 3(b)–(d) show stress–strain curves for pristine (0×), one-time reprocessed (1×), and two-times reprocessed (2×) composites for three different compositions (PP-14.5, PP-26.3, and PP-44.6). There is no significant degradation in mechanical properties, with elastic moduli that are invariant with reprocessing. Moreover, the elongation at break (ε_{break}) of all compositions shows an increase after reprocessing, with some composites also showing an improvement in UTS after each reprocess cycle. We speculate that the increase in ε_{break} is due to better connectivity of the polymer phase because of polymer flow with reprocessing that better fills the pore structure around the ceramic particles.

Reprocessing of PP through re-extrusion leads to degradation through chain scission, which degrades mechanical properties.[10] Previous work has shown that chain scission in PP can be prevented if processing temperatures are lower than 230 °C.[11] Reports on gypsum recycling has shown that the mechanical properties do not degrade after a few reprocessing cycles ($\leq 3\times$) when the water/gypsum ratio is kept constant.[46] We show that $CaSO_4$/PP composites can be reprocessed through cold sintering (at 160 °C) at least 10 times, with no degradation of mechanical properties. Fig. 4 shows that the UTS, ε_{break}, and the Young's modulus of PP-44.6 does not decrease with reprocess cycle; Fig. 4(a) and (b) show a slight increase for UTS and ε_{break}. This increase in properties is

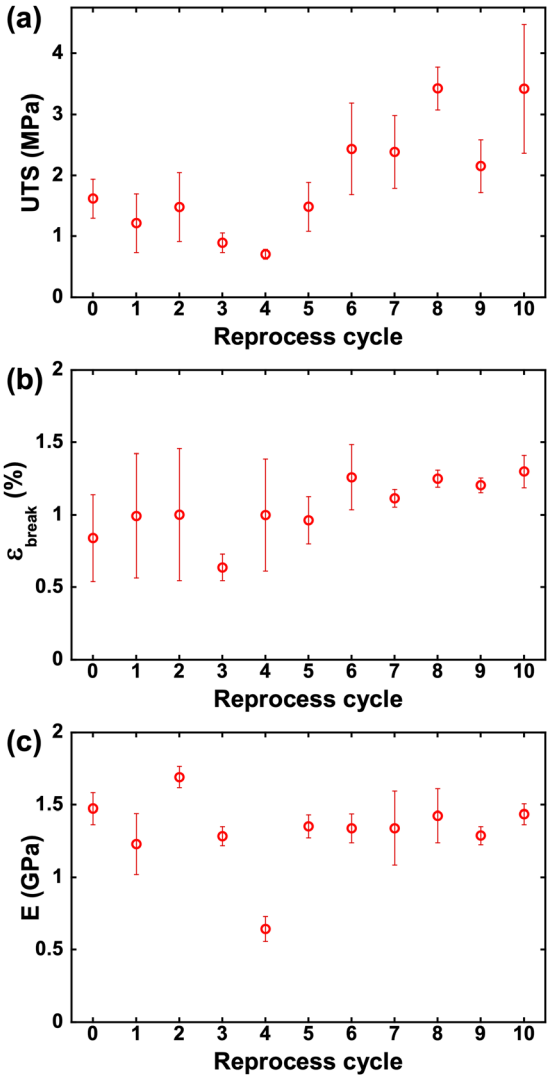

Fig. 4 Tensile properties of PP-44.6 after several reprocess cycles. (a) Ultimate tensile strength. (b) Elongation at break, and (c) Young's modulus after reprocessing.

because after several reprocessing cycles, the domains of $CaSO_4$ and PP become smaller (Table S1, ESI†). Fig. 4(c) shows a mostly invariant Young's modulus with reprocessing, except for a modest decrease in the fourth reprocessing cycle and subsequent recovery in later reprocessing. In addition, Fig. S6 (ESI†) shows FTIR spectra where there is no perceptible change in chemical structure after 10 times reprocessing. μ-CT analysis after reprocessing in Fig. S7 and Table S1 (ESI†) show that the composition and PP connectivity are consistent with reprocessing. Based on Fig. S8(a) (ESI†), the relative density of all composites remains consistent across different reprocessing steps, and the density of recycled composites is not correlated with variations in mechanical properties (Fig. S8(b)–(d), ESI†). We speculate that the smaller $CaSO_4$ domain sizes prevent crack propagation through the $CaSO_4$/PP composites. Indeed, we observe a correlation between the thickness of $CaSO_4$ domains and the UTS, as shown in Fig. 5.

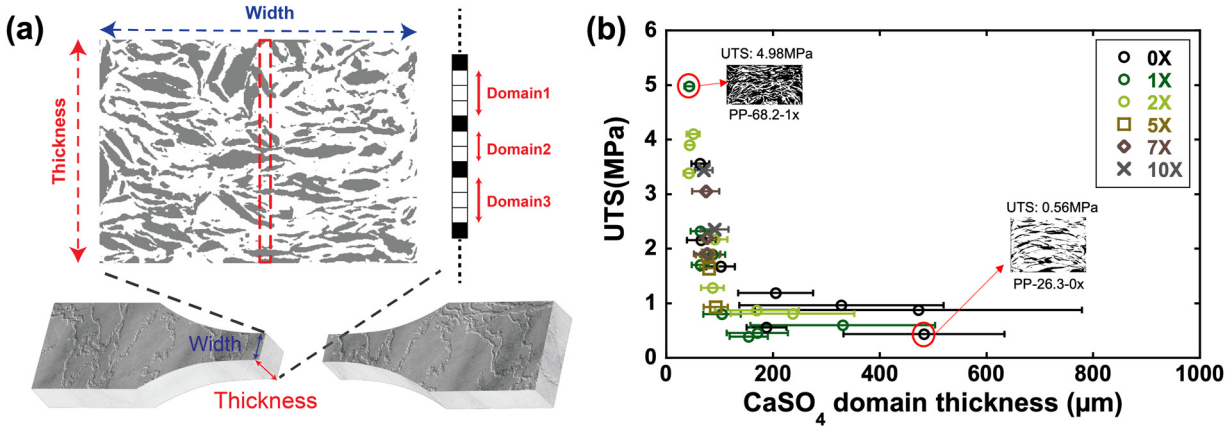

Fig. 5 Correlation between thickness of $CaSO_4$ domains and the UTS. (a) Schematic illustrating the aggregated domain size of $CaSO_4$ in the $CaSO_4$/PP composites, including how "thickness" is defined. (b) UTS *versus* $CaSO_4$ domain size in the direction of the thickness of samples that vary in composition and number of reprocessing steps.

Given the low ultimate tensile strength of $CaSO_4$, we speculate that cracks first form and rapidly propagate in $CaSO_4$ domains of $CaSO_4$/PP composites. We thus also hypothesize that there is a relationship between $CaSO_4$ domain sizes and UTS. We quantify the size of $CaSO_4$ domains along the thickness of the composite, as shown in Fig. 5(a). In Fig. 5(b), the UTS for the various samples included in this work is plotted *versus* the $CaSO_4$ domain size along the thickness of the composites. The UTS of composites is low (<1 MPa) when the average $CaSO_4$ domain size is larger than approximately 100 μm. We speculate that the larger $CaSO_4$ domain sizes provide pathways for crack propagation and decreases the UTS of the composite. In contrast, when the $CaSO_4$ domain size is smaller than 100 μm, the smaller domains reduce crack percolation and result in harder to break composites with higher UTS.

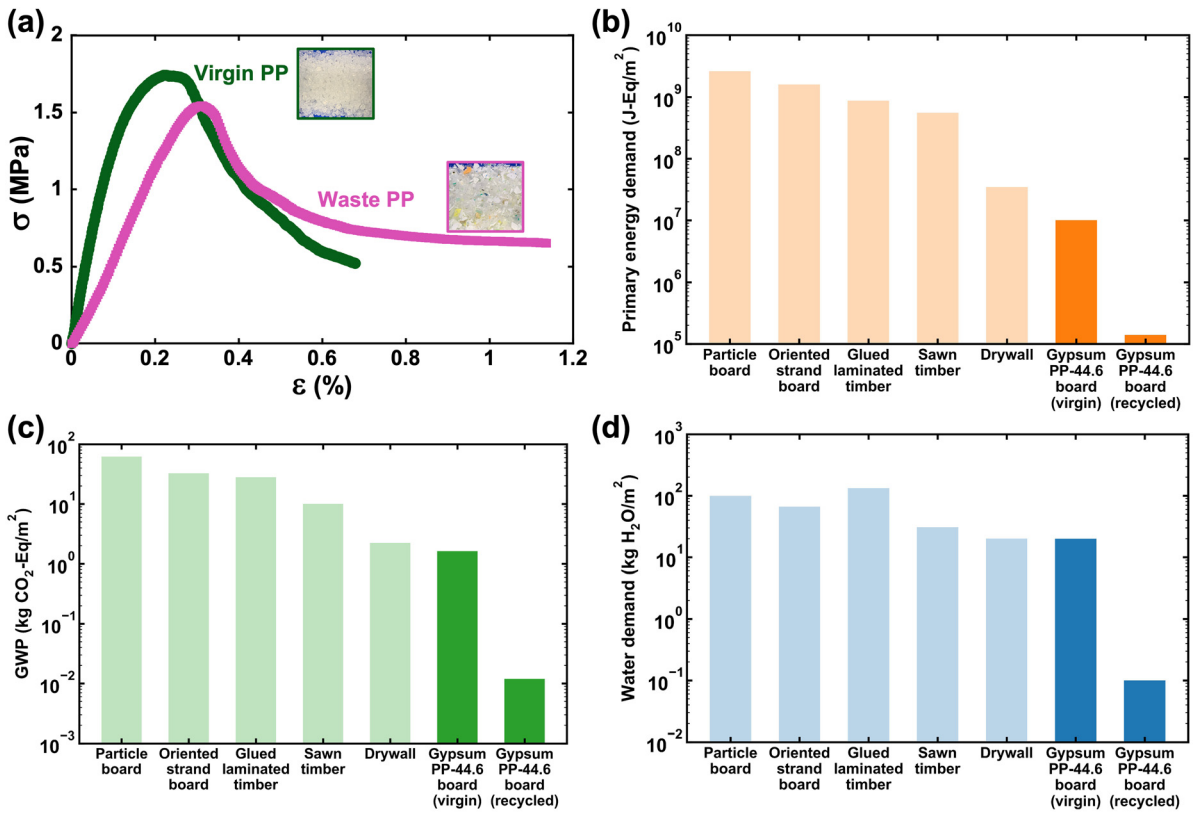

Fig. 6 (a) Representative stress–strain curves comparison between PP-44.6 (virgin PP) and Waste-PP-44.6 (waste PP) for the same composition (44.6 vol% of PP). Life cycle analysis for common construction materials for (b) primary energy demand, (c) global warming potential (GWP), and (d) water demand. For comparison, the thickness of all materials was assumed to be 12.7 mm for LCA analyses.

Upcycling waste PP and LCA analysis

To demonstrate the potential to enhance sustainability, we incorporate waste PP (post-industrial recycled PP, see Fig. S9, ESI†) to fabricate $CaSO_4$-PP composites that are analogous to those previously described. Fig. 6(a) and Table S2 (ESI†) illustrate the equivalence of Waste-PP-44.6 to the composite produced with virgin PP. The Young's modulus of Waste-PP-44.6 is slightly less than the virgin composite, but this is consistent with the rule of mixtures as the waste PP exhibits reduced mechanical performance, as illustrated in Fig. S10 and Table S3 (ESI†). Nevertheless, the UTS and elongation at break for the Waste-PP-44.6, despite the lower properties for the waste PP in comparison to virgin PP as shown in Table S3 (ESI†), are nearly identical to virgin PP-44.6. This limited impact of the properties of the polymer phase suggests that the ceramic properties can dominate the composite performance after cold sintering; this is a direct consequence of fusing the inorganic phase and leads to an intrinsic tolerance to variance in polymer properties. Thus, cold sintering of composites is well suited to incorporate waste plastic, which can vary substantially depending on the source, for the synthesis of tough composites.

We quantify the potential impact on the environment of our recyclable cold sintered composites through life cycle analyses (LCA) that include the production of the raw materials and assess the energy demand and global warming potential (GWP), as shown in Fig. 6(b) and (c). As water is used in the cold sintering process, the water demand relative to other common construction materials is shown in Fig. 6(d). Fig. 6 illustrates the environmental advantages of cold sintering relative to conventional building materials, even without recycling, although more work is needed to establish industrial-scale cold sintering processes that can be compared with established processes of other construction materials. Recycled composites significantly reduce impact, with orders of magnitude decrease across all three categories in comparison to traditional materials. Even though cold sintering requires water as a transient solvent, the amounts are modest in comparison to many of the processing steps required for common materials, such that the cold sintered recycled materials use three orders of magnitude less water than glued laminate timber (we assume zero water recovery in the cold sintered process). Quantification of environmental impact by LCA, shown in Fig. 6, highlights the impact of virgin material fabrication, the substantial benefits to recycle waste materials with low energy processes, and the potential for cold sintering to enhance circularity in the building and construction industry through recyclable composites.

Conclusions

Cold sintering can create recyclable composite materials from mixtures of PP and $CaSO_4$, which opens the door for integration of plastic and construction waste for structural composites. Furthermore, PP/$CaSO_4$ cold sintered composites exhibit mechanical properties that surpass those of hot-pressed composites. Specifically, the cold sintering process results in a 30% increase in Young's modulus, three times larger strain at break, and an eightfold increase in ultimate tensile stress (UTS). X-ray tomography reveals that, at nearly symmetric compositions, cold sintering can lead to co-continuous microstructures, where densification of both the inorganic and organic phase is achieved. We show that such composites can be directly reprocessed through mechanical means and cold sintering, with no apparent degradation in chemistry or tensile properties after reprocessing. We demonstrate the incorporation of plastic waste (post-industrial) using cold sintering, and similar resulting composite mechanical properties. The environmental impact of the reprocessed cold sintered composite is orders of magnitude less than common building materials; even with virgin feedstocks, cold sintering offers a lower energy demand and reduced global warming potential. These findings highlight the reduced environmental impact of our cold-sintered composites as a sustainable alternative to conventional construction materials. Altogether, we show that cold sintering opens the door for low-temperature processing and reprocessing of recyclable composites that can be generated from waste and thereby provide a new direction for sustainable materials.

Materials and methods

Materials

Polypropylene (PP, PP4792E1) was obtained from ExxonMobil. Calcium sulfate ($CaSO_4$, 99.9%, 325 mesh) was purchased from Sigma-Aldrich. Waste PP was obtained from EPI Recycling Solutions (Erie, PA); the PP used was a segregated homopolymer polypropylene from a packaging injection molder, which can be considered as mixed post-industrial recycled PP. The PP pellets were reduced to smaller particles using a cryomill (Retsch CryoMill) operating at 30 Hz and 77 K. After 4 min of grinding, the PP powder was fractionated by separating out the larger particles with a 35 mesh sieve and then the final particles were obtained from a 60 mesh sieve for a nominal particle size between 250 and 500 μm. $CaSO_4$ with a reported particle size of 40 μm was used directly without further processing.

We mix materials for cold sintering through sequential addition of powders, with $CaSO_4$ being introduced into the mortar first, followed by the addition of PP. The blending procedure uses spatulas to stir the two materials for approximately 15–30 s to provide a uniform distribution of both powders. Subsequently, deionized water, constituting 10 wt% of the total powder mass, was added dropwise using a pipette over the powders to uniformly wet the materials. The moistened powders were further mixed through grinding with a mortar and pestle for 1 min. The selection of a transient solvent, crucial for facilitating particle compaction and controlling dissolution and precipitation stages, led us to choose water due to its reported suitability for dissolving $CaSO_4$.[47] The 10 wt% water content was chosen to follow reported cold sintering processes.[20]

The moistened powders were loaded into a 3-part mold (316 Stainless steel) with Kapton tape (addicore, 0.06 mm) on

the top and bottom for clean release of type V tensile bars (ASTM D638). The use of 316 stainless steel molds was driven by the need for corrosion resistance, given the susceptibility of steels to corrosion from $CaSO_4$. The cold sintered temperature was 160 °C, which is near the melting point of PP (Fig. S11, ESI†). This sintering temperature achieves simultaneous cold sintering of $CaSO_4$, water evaporation, and PP flow. Lower temperatures, such as 140 °C, lead to minimal melting of PP and poor mechanical properties (Fig. S12a, ESI†) and 180 °C or 200 °C leads to leaking of PP from cold sintering molds (Fig. S12b and c, ESI†). Cold sintering took place with an applied uniaxial pressure of 200 MPa for 1 h. This pressure was chosen as the effective limit for the mold due to the lower yield strength of 316 stainless steel. Additionally, the 1 h sintering duration was determined as sufficient to reach the maximum achievable density under our processing conditions as shown in Fig. S13 (ESI†).

Mechanical properties

The tensile properties of the dogbone composites with a gauge length of 25.4 mm were determined following ASTM D638 using an Instron 5943 (100 N load cell) at 0.5 mm min^{-1}. The cross-sectional area (thickness and width) was measured with digital calipers prior to deformation. The tensile results are reported as engineering stress and strain to determine the Young's modulus, ultimate tensile stress, strain at break, and strain at yield. All compositions were tested multiple times ($n \geq 5$ except extended reprocessing where $n \geq 3$ for all cycles) for statistics.

Morphological characterization with μCT analysis

The internal structure and morphology of the composites after the tensile tests were determined using X-ray microcomputed tomography (μCT, GE v | tome | x L300 multiscale nano/μCT system) operating at 120 kV/60 μA with a voxel resolution of 7.5 μm. The difference in the electron density of PP, $CaSO_4$ and voids enables identification of composite components according to their grayscale value in AVIZO (version 2021.1, Thermo Fisher Scientific) to calculate the composition and phase connectivity in the composites.

The morphology from μCT was quantified in terms of $CaSO_4$ domain size and phase connectivity. The domain size distribution was determined through binary reconstruction as 2D slices across the gauge region by Otsu's method[48] to separate PP and $CaSO_4$ regions. The $CaSO_4$ domain sizes across the width and thickness of the gauge region provide the length for crack growth from failure of $CaSO_4$ domains. The full distribution of cord lengths was calculated in both the width and thickness in the gauge section. Code for determining the cord length is available online.[49] To address the connectivity of the phases, the original gray scale values were reconstructed into binary 3D images by application of Otsu's method.[50] These binary 3D images were analyzed with Skimage (Python) to detect each individual $CaSO_4$ connected region.

Reprocessing *via* cold sintering

After mechanical testing to failure and subsequent morphological characterization, the cold-sintered $CaSO_4$/PP tensile bars were broken into pieces and re-ground by mortar and pestle into fine powders. These powders were re-processed following the same procedure, first wetting the composite powder (10 wt% DI water) and then cold-sintered (200 MPa, 160 °C, 1 h) to a reprocessed tensile sample. This reprocessing cycle was performed multiple times to demonstrate the recyclability of these materials.

Life cycle analysis (LCA)

Life cycle analyses (LCA) of the cold sintering process was cradle-to-gate. Three impact categories, primary energy demand, global warming potential 100 (GWP-100), and water demand, were assessed with LCA. To calculate the primary energy demand and GWP-100 for the cold sintering process, a predictive energy model was established using intrinsic thermodynamic characteristics of the composite blend, and energy consumption was calculated following an approach previously described.[51] We assumed that the electricity required to power our process is pulled from the electric grid for the state of Pennsylvania. Because the process is consuming energy from the local grid, information regarding fuel mix breakdown and GWP of the grid was obtained from the EPA eGRID database.[52] Primary energy demand was calculated using the energy for raw material extraction (mining), initial raw material processing to obtain pure product, and transporting the material. LCA for the cold sintered materials developed in this work, including virgin gypsum and PP-46 composites,[53,54] were compared to other common building materials: sawn timber (softwood kiln dried),[55] particle board,[56] oriented strand board,[57] glue laminated timber,[58] and gypsum board (drywall).[54] The scope of LCA studies of common building materials used for comparison are cradle-to-gate. The impact assessment method used was the US EPA tool for reduction and assessment of chemicals and other environmental impacts (TRACI). TRACI provides characterization factors for life cycle impact assessment, industrial ecology, and sustainability metrics.[59] These factors quantify the potential impacts that process inputs and outputs have on selected impact categories in equivalence units. We assume the operational conditions for cold sintering processes are the same when scaling up. Additionally, we assume building products from cold sintering to be 12.7 mm thick, which is an industry standard size, for comparison between materials.

Author contributions

Po-Hao Lai: conceptualization, experimentation, coding for morphological characterization, and writing – review & editing. Shelby L. Hall: conducted the life cycle assessment (LCA) analysis, and contributed to writing, review, and editing. Yi-Chen Lan: conceptualization and supervision. Jia-Ruey Ai: conceptualization and supervision. Arian Jaberi: provided guidance and instruction for the tensile experiment. Amir Sheikhi: provided supervision. Rui Shi: conducted the LCA analysis, contributed to writing, review, and editing, and provided supervision. Bryan D. Vogt: conceptualization, writing – review & editing, supervision,

and acquisition of funding. Enrique D. Gomez: conceptualization, writing – review & editing, supervision, and acquisition of funding.

Conflicts of interest

The authors declare no conflicts of interest.

Acknowledgements

The authors gratefully acknowledge experimental support from Gino Lee Tambourine, Nichole M Wonderling, Beth Anna Last, Shang-Lin Yeh, Zaman Ataie, Sara Jaye Muller, Timothy Stecko, Hsiao-Han Tseng and Masoud Ghasemi. Funding from the Pennsylvania State University and National Science Foundation under Award CBET-2134643 is acknowledged. Acknowledgement is made to the donors of the American Chemical Society Petroleum Research Fund for partial support of this research under Award 60974-ND7. The authors thank Pete Previte and Bob Bylone at the Pennsylvania Recycling Markets Center as well as Kurt Duska at Engineered Plastics LLC for their help in procuring waste polypropylene.

References

1 R. Geyer, J. R. Jambeck and K. L. Law, *Sci. Adv.*, 2017, **3**, e1700782.
2 W. C. Li, H. F. Tse and L. Fok, *Sci. Total Environ.*, 2016, **566–567**, 333–349.
3 C. M. Rochman, M. A. Browne, B. S. Halpern, B. T. Hentschel, E. Hoh, H. K. Karapanagioti, L. M. Rios-Mendoza, H. Takada, S. Teh and R. C. Thompson, *Nature*, 2013, **494**, 169–171.
4 K. Ragaert, L. Delva and K. Van Geem, *Waste Manag.*, 2017, **69**, 24–58.
5 J. Hopewell, R. Dvorak and E. Kosior, *Philos. Trans. R. Soc., B*, 2009, **364**, 2115–2126.
6 M. Pavuk, in *Dioxins and Health*, ed. A. Schecter, T. Gasiewicz, 2nd edn, 2003.
7 S. Kheirabadi and A. Sheikhi, *Curr. Opin. Green Sustainable Chem.*, 2022, **38**, 100695.
8 J. Aurrekoetxea, M. A. Sarrionandia, I. Urrutibeascoa and M. L. Maspoch, *J. Mater. Sci.*, 2001, **36**, 2607–2613.
9 J. M. Garcia and M. L. Robertson, *Science*, 2017, **358**, 870–872.
10 O. I. Nkwachukwu, C. H. Chima, A. O. Ikenna and L. Albert, *Int. J. Ind. Chem.*, 2013, **4**, 1–13.
11 H. Sardon and A. P. Dove, *Science*, 2018, **360**, 380–381.
12 F. Vilaplana and S. Karlsson, *Macromol. Mater. Eng.*, 2008, **293**, 274–297.
13 I. Vollmer, M. J. Jenks, M. C. Roelands, R. J. White, T. van Harmelen, P. de Wild, G. P. van Der Laan, F. Meirer, J. T. Keurentjes and B. M. Weckhuysen, *Angew. Chem., Int. Ed.*, 2020, **59**, 15402–15423.
14 A. Gallego-Schmid, H.-M. Chen, M. Sharmina and J. M. F. Mendoza, *J. Cleaner Prod.*, 2020, **260**, 121115.
15 J. Andrews, D. Button and I. M. Reaney, *Johnson Matthey Technol.*, 2020, **64**, 219–232.
16 J. Guo, X. Zhao, T. Herisson De Beauvoir, J. H. Seo, S. S. Berbano, A. L. Baker, C. Azina and C. A. Randall, *Adv. Funct. Mater.*, 2018, **28**, 1801724.
17 J. Guo, R. Floyd, S. Lowum, J.-P. Maria, T. Herisson de Beauvoir, J.-H. Seo and C. A. Randall, *Annu. Rev. Mater. Res.*, 2019, **49**, 275–295.
18 H. Guo, T. J. Bayer, J. Guo, A. Baker and C. A. Randall, *Scr. Mater.*, 2017, **136**, 141–148.
19 S. Grasso, M. Biesuz, L. Zoli, G. Taveri, A. I. Duff, D. Ke, A. Jiang and M. J. Reece, *Adv. Appl. Ceram.*, 2020, **119**, 115–143.
20 J.-P. Maria, X. Kang, R. D. Floyd, E. C. Dickey, H. Guo, J. Guo, A. Baker, S. Funihashi and C. A. Randall, *J. Mater. Res.*, 2017, **32**, 3205–3218.
21 A. Galotta and V. M. Sglavo, *J. Eur. Ceram. Soc.*, 2021, **41**, 1–17.
22 T. Yu, J. Cheng, L. Li, B. Sun, X. Bao and H. Zhang, *Front. Chem. Sci. Eng.*, 2019, **13**, 654–664.
23 A. Ndayishimiye, S. H. Bang, C. J. Spiers and C. A. Randall, *J. Eur. Ceram. Soc.*, 2023, **43**, 1–13.
24 J. Guo, H. Guo, A. L. Baker, M. T. Lanagan, E. R. Kupp, G. L. Messing and C. A. Randall, *Angew. Chem.*, 2016, **128**, 11629–11633.
25 J. Guo, S. S. Berbano, H. Guo, A. L. Baker, M. T. Lanagan and C. A. Randall, *Adv. Funct. Mater.*, 2016, **26**, 7115–7121.
26 W. Lee, C. K. Lyon, J.-H. Seo, R. Lopez-Hallman, Y. Leng, C.-Y. Wang, M. A. Hickner, C. A. Randall and E. D. Gomez, *Adv. Funct. Mater.*, 2019, **29**, 1807872.
27 S. Funahashi, H. Z. Guo, J. Guo, A. L. Baker, K. Wang, K. Shiratsuyu and C. A. Randall, *J. Am. Ceram. Soc.*, 2017, **100**, 3488–3496.
28 T. Zhou, Y. Liu, P. Cao, J. Du, Z. Lin, R. Wang, L. Jin, L. Lian and V. G. Harris, *Adv. Electron. Mater.*, 2020, **6**, 2000868.
29 V. A. González-González, G. Neira-Velázquez and J. L. Angulo-Sánchez, *Polym. Degrad. Stab.*, 1998, **60**, 33–42.
30 A. Jansson, K. Möller and T. Gevert, *Polym. Degrad. Stab.*, 2003, **82**, 37–46.
31 T. Thiounn and R. C. Smith, *J. Appl. Polym. Sci.*, 2020, **58**, 1347–1364.
32 U.S. EPA: Construction and Demolition Debris: Material-Specific Data, **https://www.epa.gov/facts-and-figures-about-materials-waste-and-recycling/construction-and-demolition-debris-material**, (accessed April 10, 2023).
33 S. M. Pinheiro and G. Camarini, *Int. J. Eng. Technol.*, 2015, **7**, 215.
34 R. H. Geraldo, S. M. Pinheiro, J. S. Silva, H. M. Andrade, J. Dweck, J. P. Gonçalves and G. Camarini, *J. Cleaner Prod.*, 2017, **164**, 288–300.
35 E. Martin, D. Leguillon, O. Sevecek and R. Bermejo, *Eng. Fract. Mech.*, 2018, **201**, 167–175.
36 S. Seshadri and K. Y. Chila, *J. Am. Ceram. Soc.*, 1987, **70**, C-242–C-244.
37 L. Li, H. Yan, W. B. Hong, S. Y. Wu and X. M. Chen, *J. Eur. Ceram. Soc.*, 2020, **40**, 4689–4693.

38 K. Nur, M. Zubair, J. S.-L. Gibson, S. Sandlöbes-Haut, J. Mayer, M. Bram and O. Guillon, *J. Eur. Ceram. Soc.*, 2022, **42**, 512–524.
39 T. Matsumoto and H. Mihashi, *J. Adv. Concr. Technol.*, 2003, **1**, 335–340.
40 M. Lan, J. Zhou and M. Xu, *Front. Mater.*, 2021, **8**, 775188.
41 R. Madandoust, M. M. Ranjbar, R. Ghavidel and S. Fatemeh Shahabi, *Mater. Des.*, 2015, **83**, 284–294.
42 M. H. Al-Saleh and U. Sundararaj, *Composites, Part A*, 2011, **42**, 2126–2142.
43 F. Liu, K. Xu, W. Ding, Y. Qiao and L. Wang, *Cem. Concr. Compos.*, 2021, **123**, 104196.
44 I. Soroka and P. J. Sereda, *J. Am. Ceram. Soc.*, 1968, **51**, 337–340.
45 P. Tesárek, T. Plachý, A. Hájková, P. Padevět and M. Polák, *Proceeding of Latest Trends on Engineering Mechanics, Structures, Engineering Geology*, WSEAS, Athens, 2010, 413417.
46 C. Zhu, J. Zhang, W. Yi, W. Cao, J. Peng and J. Liu, *Constr. Build. Mater.*, 2018, **173**, 540–549.
47 K. Ishikawa, *Materials*, 2010, **3**, 1138–1155.
48 S. L. Bangare, A. Dubal, P. S. Bangare and S. T. Patil, *Int. J. Appl. Eng. Res.*, 2015, **10**, 21777–21783.
49 Composite CT thickness calculation, **https://github.com/Albert840529/Composite_CT_Thickness_calculation/blob/main/CT_Image_Thickness_Calculation.ipynb**.
50 J. Zhang and J. Hu, Presented in part at the 2008 International Conference on Computer Science and Software Engineering, 2008.
51 T. Ibn-Mohammed, C. A. Randall, K. B. Mustapha, J. Guo, J. Walker, S. Berbano, S. C. L. Koh, D. Wang, D. C. Sinclair and I. M. Reaney, *J. Eur. Ceram. Soc.*, 2019, **39**, 5213–5235.
52 United States Environmental Protection Agency **https://www.epa.gov/egrid** 2023.
53 K. C. Mike Levy and P. Muhuri, *Cradle-to-Gate Life Cycle Analysis of Polypropylene (PP) Resin*, Franklin Associates American Chemistry Council, 2021.
54 J. M. Lindita Bushi, *An Industry Average Cradle-to-Gate Life Cycle Assessment of 1/2'' Lightweight and 5/8'' Type X Conventional Gypsum Board for the USA and Canadian Markets Gypsum Association Athena Sustainable Materials Institute* 2020.
55 M. Puettmann, E. Oneil, M. Milota and L. Johnson, *Cradle-to-Gate Life Cycle Assessment of Softwood Lumber Production from the Southeast, Consortium for Research on Renewable Industrial Materials* 2012.
56 M. Puettmann, E. Oneil and J. Wilsom, *Cradle-to-Gate Life Cycle Assesment of US Particleboard Production Consortium for Research on Renewable Industrial Materials* 2013.
57 M. Puettmann, D. Kaestner and A. Taylor, *CORRIM REport - Module E Life Cycle Assessment of Oriented Strandboard (OSB) Production Consortium for Research on Renewable Industrial Materials* 2016.
58 M. Puettmann, E. Oneil and L. Johnson, *Gradle-to-Gate Life Cycle Assesment of Glue-Laminated Timbers Production from the Pacific northwest, Consortium for Research on Renewable Industrial Materials* 2013.
59 J. C. N. Bare, G. A. Pennington and D. W. McKone, Tool for Reduction and Assesment of Chemicals and Other Environmental Impacts **https://www.epa.gov/chemical-research/tool-reduction-and-assessment-chemicals-and-other-environmental-impacts-traci**, (accessed June 26, 2023).

